Research Article | Vol. 27, No. 20 | 30 Sep 2019 | OPTICS EXPRESS 28816
Optics EXPRESS

Stochastic polarization switching induced by optical injection in bimodal quantum-dot micropillar lasers

ELISABETH SCHLOTTMANN,[1] DAVID SCHICKE,[2] FELIX KRÜGER,[1] BENJAMIN LINGNAU,[2,3] CHRISTIAN SCHNEIDER,[4] SVEN HÖFLING,[4,5] KATHY LÜDGE,[2] XAVIER PORTE,[1,6] AND STEPHAN REITZENSTEIN[2,*]

[1] *Institut für Festkörperphysik, Optoelectronics and Quantum Devices, Technische Universität Berlin, Hardenbergstraße 36, 10623 Berlin, Germany*
[2] *Institut für Theoretische Physik, AG Nichtlineare Laserdynamik, Technische Universität Berlin, Hardenbergstraße 36, 10623 Berlin, Germany*
[3] *University College Cork, Department of Physics, and Tyndall National Institute, Cork, Ireland*
[4] *Technische Physik, Universität Würzburg, Am Hubland, 97074 Würzburg, Germany*
[5] *SUPA, School of Physics and Astronomy, University of St Andrews, St Andrews, KY16 9SS, UK*
[6] *Now with: FEMTO-ST/Optics Dept., UMR CNRS 6174, Univ. Bourgogne Franche-Comté, 15B avenue des Montboucons, 25030 Besançon Cedex, France*
[*] *stephan.reitzenstein@physik.tu-berlin.de*

Abstract: Mutual coupling and injection locking of semiconductor lasers is of great interest in non-linear dynamics and its applications for instance in secure data communication and photonic reservoir computing. Despite its importance, it has hardly been studied in microlasers operating at μW light levels. In this context, vertically emitting quantum dot micropillar lasers are of high interest. Usually, their light emission is bimodal, and the gain competition of the associated linearly polarized fundamental emission modes results in complex switching dynamics. We report on selective optical injection into either one of the two fundamental mode components of a bimodal micropillar laser. Both modes can lock to the master laser and influence the non-injected mode by reducing the available gain. We demonstrate that the switching dynamics can be tailored externally via optical injection in very good agreement with our theory based on semi-classical rate equations.

1. Introduction

Cavity-enhanced micro- and nanolasers are state-of-the-art solid state nanophotonic devices based on dielectric or plasmonic resonators [1–5]. Combined with a suitable low-dimensional gain medium, such resonators show very interesting physical properties like few-emitters lasing [6, 7], thresholdless lasing [8] and spiking dynamics [9]. Their exciting properties emerge from the combination of low-dimensional gain centers and cavities with very low mode volumes and high quality factors (Q) which enable enhanced light-matter coupling in the regime of cavity quantum electrodynamics (cQED) [10] and lead to high spontaneous emission factors (β-factor) [11]. Such non-classical characteristics make these nanophotonic devices especially appealing for applications in nanotechnology as, for instance, resonant excitation source for the generation of indistinguishable photons [12].

Nonlinear dynamics induced by optical injection are well-known in standard semiconductor lasers with mW emission power [13]. Injection into two-state lasers has also been investigated intensively in the past [14, 15] and showed interesting dynamics that can be useful in applications like all optical gating [16] or all-optical memory [17]. The opportunity to use semiconductor lasers as test-bed systems to perform in-depth studies of non-linear dynamics has led to exciting results and novel applications [18], a successful approach that we aim to reproduce in semiconductor

#368891 https://doi.org/10.1364/OE.27.028816
Journal © 2019 Received 30 May 2019; revised 2 Aug 2019; accepted 2 Aug 2019; published 24 Sep 2019

Optics EXPRESS

micro- and nanolasers. In this context, optical injection and coupling are successful approaches to generate highly complex dynamics in semiconductor lasers [14,15]. Particularly interesting complex dynamics are presented by vertically emitting lasers, where polarization chaotic-switching dynamics can be induced by optical injection [19, 20], with potential applications in microwave generation [21] and in all-optical flip-flop photonic integrated devices [22–24].

Enabled by the huge progress in the realization of microlasers it has become feasible to extend these kind of investigation to the widely unexplored quantum regime of non-linear dynamics. Among existing micro- and nanolasers, quantum dot (QD) micropillar lasers are of particular interest for related studies of non-linear dynamics at ultra-low light levels. These lasers are rather robust, can be driven electrically and provide efficient in- and out-coupling of light normal to the sample surface. In these vertically emitting microlasers the gain is provided by only tens to a few hundreds of QDs coupled to the laser mode [25]. Rather small threshold powers together and cavity photon numbers on the order of 10 - 100 make micropillar lasers excellent candidates to explore nonlinear laser dynamics in the few-photon limit with future prospects in the quantum regime of optical feedback [26, 27] and synchronization [28–30]. The application of VCSELs has become important for optical interconnects due to their large modulation bandwidth and energy efficiency. Recently, a new record in both has been established for a bimodal VCSEL used as spin-laser [31]. Smaller apertures have been advantageous on the modulation bandwidth [32] and the Purcell effect is expected to further enhance the speed of micro- and nanolasers [33]. In this regard small-scale microlasers are of particular interest to push the limits of spin-injected lasers [31] to the regime of cQED with enhanced light-matter interaction and tight mode confinement. As such they allow for geometric tailoring of the mode splitting and potentially even lower heat-to-data ratios. Similarly, dense arrays of diameter-tuned microlasers with high spectral homogeneity [34–36] have high potential to enable powerful photonic reservoir computing based on the diffractive coupling of optically injected microlasers. Interestingly, despite these appealing applications and the fundamental interest in exploring the physics of micro- and nanoscale lasers the injection locking behavior of cavity-enhanced lasers is still widely unexplored.

A first study on the effects of optical injection in single mode micropillar lasers already unveiled interesting phenomena like partial locking, which is caused by the high values of the β-factor in such devices [37]. Vertically emitting semiconductor lasers provide an additional degree of freedom, namely the bimodal behavior associated with two linearly polarized components of the fundamental cavity mode. The orthogonally polarized modes compete for the common optical gain provided by the QDs in the active layer, and typically one of the two modes wins the competition and undergoes lasing in detriment of its counterpart [38]. The continuous competition between both polarization modes at suitable bias points is reflected in switching dynamics [39]. The intensity noise in our cavity-enhanced QD micropillar lasers is 2-3 orders of magnitude higher compared to VCSELs. This potentially increases the impact of stochastic polarization switching between the modes in cavity-enhanced QD micropillar lasers. Complex chaotic dynamics in VCSELs [40] or delay-coupled lasers [41] finds potential applications in random number generation [42] and secure data communications [43]. However, the underlying dynamical processes are of deterministic origin in chaotic lasers [44], and thus may require accurate dynamics tailoring, digital post-processing or complex optical setups to achieve high-quality uncorrelated random numbers. In contrast, randomness generation based on quantum-fluctuations in QD micropillar lasers could produce analogous results with a simpler approach by taking advantage of enhanced stochastic noise in these high-β emitters. In fact, the ongoing trend of miniaturization of nanophotonic devices, naturally goes along with an increase of the relative strength of spontaneous emission. Our results show that for future applications of microlasers where such stochastic switching would be undesirable, optical injection provides a way to suppress it.

Optics EXPRESS

In this paper, we explore the effects of external optical injection in the emission of the two competing modes, identifying the spectral and dynamical changes in the micropillar laser's emission.

By changing the polarization of the optical injection, we can selectively perturb one of the two linearly polarized laser modes. We particularly focus on the switching characteristics of the bimodal emission, which we find to be strongly enhanced under optical injection to the non-lasing mode. The stochastical switching is experimentally verified by cross correlation measurements and numerical calculations give further insides to the switching character by time series.

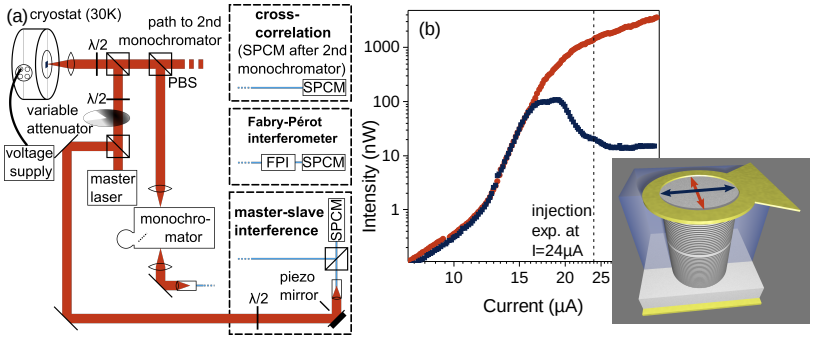

Fig. 1. (a) Experimental setup: The master laser is optically injected in the electrically driven micropillar laser. After spectral filtering using a monochromator, the micropillar emission is analyzed by either CCD, a Fabry-Pérot interferometer, a fiber-coupled cross-correlation configuration, or by interference measurements of master and microlaser emission. (b) Input-output characteristics of both micropillar modes. The SM (red) shows the typical s-shaped behavior of high-β microlasers while the WM (dark blue) first increases after threshold and reaches a maximum around 20 μA before it decreases in intensity. Inset: Schematic view of an electrically driven QD-micropillar laser. The polarization of the two orthogonal fundamental micropillar modes are indicated by the red and blue arrows.

2. Experimental setup

We report on injection locking experiments that were performed on electrically driven QD micropillar lasers realized by epitaxial growth of planar microcavity structures and subsequent processing of micropillar cavities. Details of the sample manufacturing process are given in the Appendix.

The injection locking experiments on bimodal QD-micropillar lasers were performed using the experimental setup depicted in Fig. 1(a). To achieve lasing emission, the sample is cooled down to cryogenic temperatures T = (30.00 ± 0.01) K in a temperature controlled He-flow cryostat. The electrically contacted microlasers are driven using a DC current source and the emitted light is collected and collimated by an aspheric lens with a numeric aperture of NA = 0.5. The electroluminescence signal is then dispersed by a monochromator with a focal length of 75 cm and detected by a thermoelectric-cooled Si charge-coupled device (CCD) camera with an overall spectral resolution of 27 μeV. The intensity is additionally measured by a power meter to specify the intensity in units of nW. High resolution spectra are obtained by using a Fabry-Perot interferometer (FPI) with a spectral resolution of 100 MHz and a free spectral range of 7.5 GHz.

As indicated in Fig. 1(a) polarization optics ($\lambda/2$ waveplates and a polarizing beam splitter, PBS) are used to selectively address and detect the desired microlaser polarization mode, respectively. In addition to the exclusive detection of one mode, the extended detection scheme is used to measure the cross-correlation between both micropillar modes. For this purpose, we combine a $\lambda/2$ wave-plate and a PBS to direct the light from the two modes selectively towards

Optics EXPRESS

two monochromators with attached single photon counting modules (SPCMs) each having a time resolution of 40 ps. The tunable master laser used for optical injection of the microlaser has a wavelength range from 875 nm to 940 nm and a tuning step size between 0.08 and 0.40 GHz. The master laser head possesses a built-in optical isolator. We select the polarization of the master laser via a second $\lambda/2$ waveplate in the excitation path. The injection locking effects are studied from the optical spectra of the micropillar laser and also via recording the amplitude of the interference signal between master and micropillar laser.

3. Experimental and numerical results

After presenting the pre-characterization of the bimodal QD micropillar laser, the injection locking characteristics of both modes under optical injection are discussed. In the following, the switching dynamics are reviewed by means of time series and cross correlation.

The input-output characteristic of the micropillar laser is presented in Fig. 1(b). The orthogonally polarized emission modes emit at 898.5 nm and have a spectral splitting of 47 μeV = 11 GHz. Both modes show a linear increase in output power at low injection currents in the spontaneous emission regime. At the threshold of about $I_{\mathrm{th}} = 12$ μA, the emission intensity of both modes starts to increase superlinearly due to the onset of stimulated emission. Above 16 μA a different behavior is observed for both modes: The intensity of the strong mode (SM, red) continues to increase and the standard s-shaped input-output characteristics of high-β microlasers is formed [45]. However, the weak mode (WM, dark blue), after a constant section, starts to decrease at $I \approx 19$ μA and eventually reaches a stable intensity level. This peculiar intensity dependence is typical for bimodal QD-microlasers and is attributed to the competition of both laser modes for the same gain medium. It indicates that the SM couples more effectively to the QDs in the active layer and wins the gain competition [38]. The intermediate region with comparable output powers of both modes is indicative of potential stochastic mode switching between the two polarized modes [39].

Based on the characterization presented in Fig. 1 we investigate the polarization dependent injection locking behavior of the bimodal QD microlaser. We explore how the coupling of the modes influences the emission properties of the micropillar laser under optical injection into the strong mode or into the weak mode, orthogonally polarized with respect to the first one. The studies were performed at an injection current of 24 μA, i.e. at a bias point at which we expect pronounced gain-coupling and mode-interaction effects [39]. The linewidth (FWHM) of the modes is here $\nu_{\mathrm{SM}} = 0.77$ μeV = 0.19 GHz and $\nu_{\mathrm{WM}} = 8.2$ μeV = 2.0 GHz. Figs. 2 (a) and 2 (b) depict the corresponding experimental locking cones of the SM and the WM as a function of the effective injection strength K_{eff}, under injection into the SM (left panels) and WM (right panels), respectively.

The injection strength is defined as $K_{\mathrm{exp}} = \sqrt{P_{\mathrm{master}}/P_{\mathrm{microlaser}}}$ where $P_{\mathrm{microlaser}}$ is the total power of WM and SM. The injected laser signal is partly reflected on the upper facet of the micropillar, leading to non-ideal optical coupling efficiency. The effective injection strength K_{eff} is thus lower than K_{exp}, with the corresponding conversion factor calculated via matching the experimental and simulated locking widths. We obtain $K_{\mathrm{eff}} = K_{\mathrm{exp}}/(10.8 \pm 1.8)$. The detuning is defined as $\Delta = \nu_{\mathrm{master}} - \nu_{\mathrm{microlaser}}$. As depicted in the lower detection frame of Fig. 1(a) master and microlaser signal are superimposed and interfere. The resulting signal is fitted with $f(x) = y_0 + A \cdot \sin(ax + b)$. The constant y_0 corresponds to the master laser CW component and the interference amplitude A corresponds to the phase-locking strength and is plotted in color code to achieve the experimental locking cones depicted in Fig. 2(a) and 2(b). The simulated locking cone shows the time-averaged microlaser intensity. The color code of each locking cone is normalized to its maximum interference. For injection into the SM, the master laser was set to its corresponding polarization angle (153 deg. in our setup) and the injection power was varied between $K_{\mathrm{eff}} \in [0.08, 0.18]$.

Optics EXPRESS

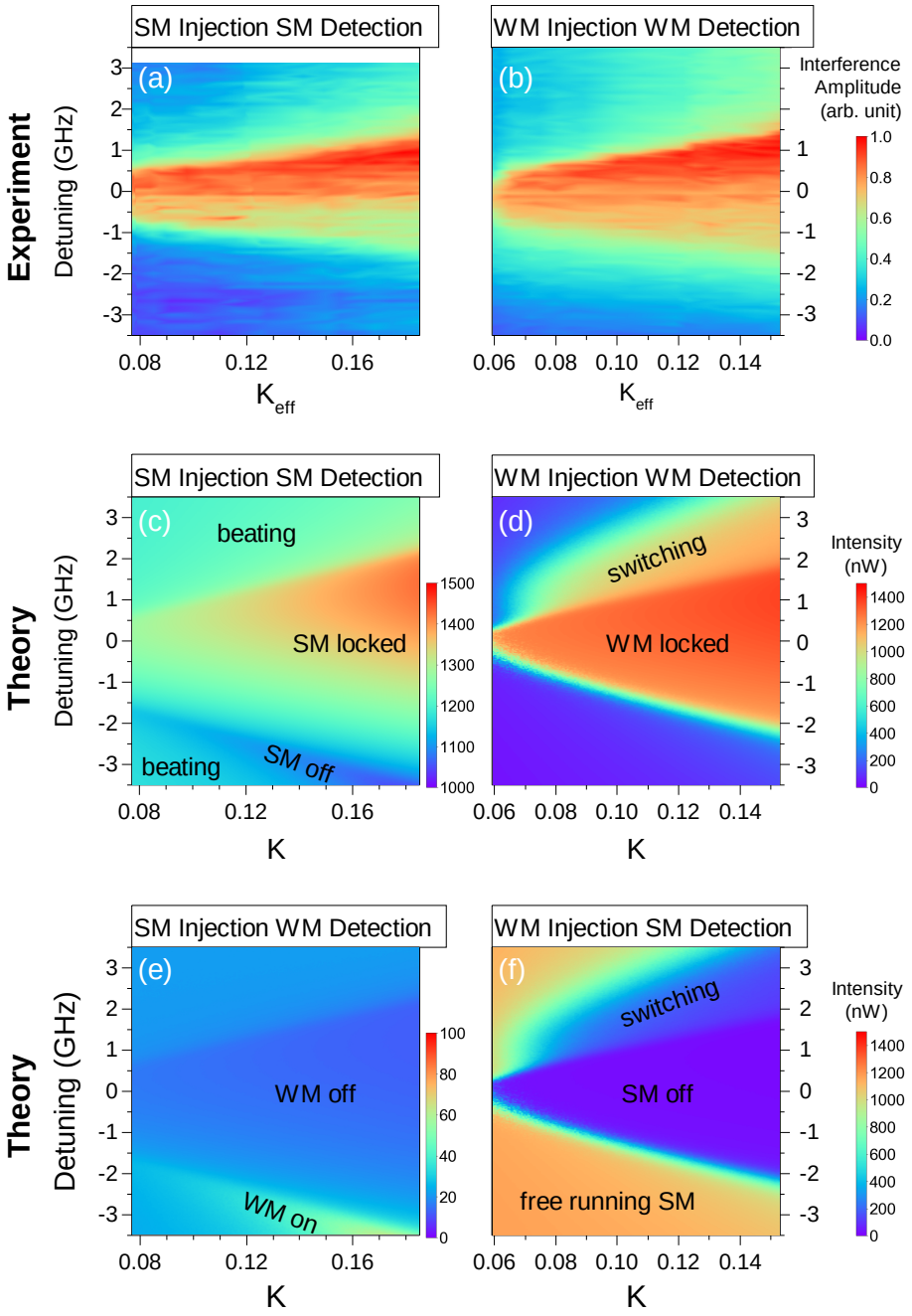

Fig. 2. (a) and (b): Experimental phase locking cones obtained with interference of master and microlaser signals. The color scale in (a) and (b) is normalized to the maximum interference amplitude, respectively. (c) - (f): Theoretical mean intensities of the two modes emitted from the micropillar laser as a function of detuning $\Delta = \nu_{\text{master}} - \nu_{\text{microlaser}}$ and injection strength (middle and bottom panels) under injection in the SM (a, c, e) and WM (b, d, f) for ±3.5 GHz detuning range.

Optics EXPRESS

The resulting locking cone in Fig. 2(a) shows a locking range with a K_{eff}-dependent width between 1.5 to 3.5 GHz. Upon crossing the locking boundary, the SM undergoes a continuous unlocking transition, returning to its free-running frequency. For high injection power, i.e. high K_{eff}, the amplitude is reduced for negative detuning (greenish area). As shown in the input-output characteristics in Fig. 1(b), the WM does not complete the transition to lasing. Nevertheless, when the master laser signal is injected into the weak mode by rotating its polarization parallel to the WM, it is possible to phase-lock the WM. This is presented in Figs. 2(b) and 2(d). This locking cone of the WM exhibits several differences compared to the strong mode dynamics. While the locking cone of the SM extends to zero injection strength with continuously shrinking locking width, the locking cone in the WM disappears below an injection strength $K_{\text{eff}} \lesssim 0.06$. This is due to the difference in gain between the WM and SM, which has to be overcome by the injected signal before the WM can start lasing. Importantly, these observations, namely the existence of the locking cone, indicate that the optical injection can drive the non-lasing mode of the microlaser into the lasing regime [46].

In order to gain a deeper understanding of the observed dynamics and perform comprehensive parameter studies, we employ theoretical simulations of the injected laser dynamics. The theoretical framework is based on our previously employed semi-classical rate equation approach [30,37,39] (see the Appendix for details). The locking dynamics observed in Figs. 2(c)- 2(f) nicely resembles what is expected for injected bimodal lasers. The difference to conventional lasers is the much larger amount of spontaneous emission noise which leads to smooth transitions between the dynamic regimes. There is a minor asymmetry of the locking cones which stems from the amplitude-phase coupling well-known in semiconductor lasers [47], leading to a gain-dependent refractive index and a dynamical shift of the lasing frequency. The simulated WM intensity in Fig. 2(d) is enhanced outside the locking cone for positive detuning. Simultaneously, the strong mode in Fig. 2(f) is not fully suppressed, but reduced in intensity. Emission on both modes can be caused by switching dynamics.

In addition to measurements of the phase locking in Figs. 2(a) and 2(b) and the characterization of the emission dynamics in Figs. 2(c)-2(f), we investigate the spectral properties of the micropillar modes by means of a high-resolution FPI. Emission from the next FPI order (FSR = 7.5 GHZ) and non-sufficiently suppressed peaks from the orthogonal polarization are visible in some spectra in Fig. 2. Heatmaps for the output power of both modes under optical injection into either mode are shown in Fig. 3. In the locking region between $\approx \pm 1$ for the case of SM injection, the SM can be clearly seen to lock to the injected signal. At the boundaries of the locking range with a detuning of about ± 1.0 GHz optical injection of the SM reveals classically expected frequency pulling towards the master laser frequency. Outside of the locking region for detuning exceeding $\approx \pm 1$ GHz, partial injection locking appears as a characteristic feature of high-β microlasers [37]. In this regime the micropillar laser is reduced in intensity, and despite enhancing the master laser, it is partially still emitting at its solitary frequency.

Interestingly, also the non-injected WM is affected by injection locking to the orthogonal mode as can be seen in Fig. 3(c), where the WM intensity is plotted under optical injection into the SM. The two narrow diagonal (vertical) features correspond to incompletely suppressed emission of the master laser (SM) from the next order of the FPI. The here discussed peak is the WM located at a relative energy of 0 GHz with a linewidth of ~ 2 GHz. While the central energy of the emission is not changed, the intensity is strongly reduced between ±1 GHz. In this region, the SM is fully locked to the master laser and, thus, couples more effectively to the gain. However, outside of the locking cone, the WM increases in intensity for negative detuning between -1 and -2 GHz. In this region, the injected signal destructively interferes with the SM field. This reduces the coupling between the SM and the gain medium, which in return leaves more gain for the WM becoming brighter. This latter result is in good agreement with the insights from theory presented in Fig. 2(e). The emergence of laser emission of the non-injected mode, i.e. the

Optics EXPRESS

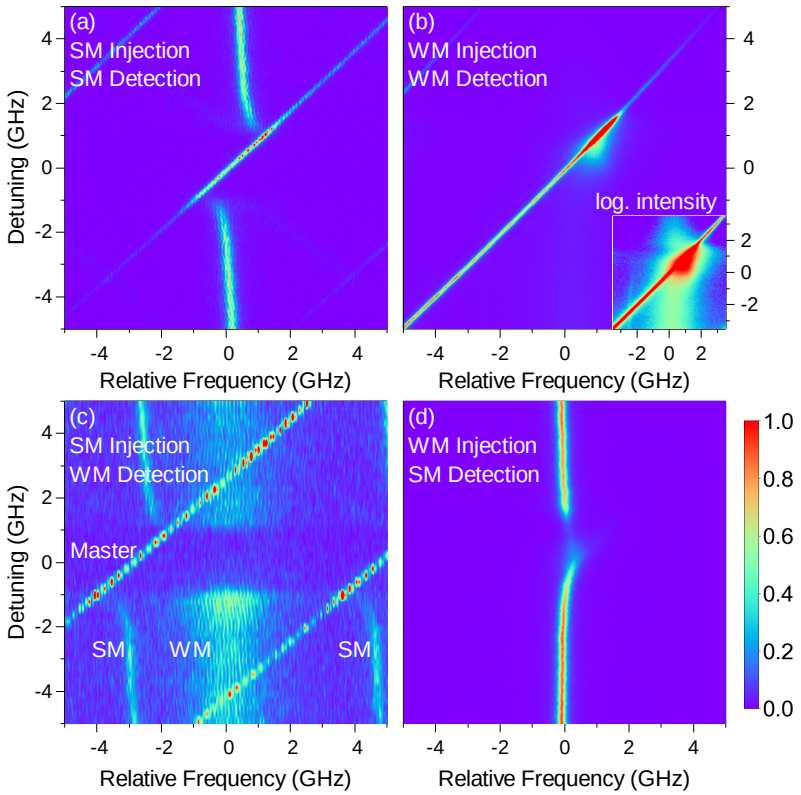

Fig. 3. Experimental intensity heatmaps measured with an FPI for spectra with a detuning range between ± 5 GHz. For injection into the SM (left panels) and WM (right panels) at $K_{\mathrm{eff}} = 0.12$ ($K_{\mathrm{eff}} = 0.066$). The response of the SM (a) and WM (c) are shown. In panel (a) the SM is clearly locked for a detuning within ± 1 GHz, where the master laser's intensity gets strongly enhanced. The broad WM in the center (c) is suppressed in the locking range and is increased at the boundary for negative detuning. The narrow peaks are the incompletely surpressed SM and master laser. In panel (b) the injected WM shows a smaller locking region compared to the corresponding situation for the SM in panel (a), and similar to panel (c) the SM is suppressed (panel (d)). The inset shows the data with logarithmic intensity scale and visualizes the broad WM.

detection of WM lasing for negatively detuned SM injection, see Fig. 2(e) and Fig. 3(c), was also experimentally observed in conventional two mode lasers [14] and explained by the underlying transcritical bifurcation [15, 17]

Figs. 3(b) and 3(d) presents experimental data recorded under optical injection into the WM. Here, panel 3(c) shows the WM spectra, while the signal of the non-injected SM is plotted in Fig. 3(d). The optical spectra confirm the results previously discussed with respect to the locking cones in Figs. 2(b), 2(d) and 2(f). The WM, which, without injection, is not operating in the lasing regime and is almost not visible outside the locking region, nevertheless locks to the master laser in a detuning range of [0.3, 1.8] GHz as verified by the associated strongly enhanced intensity in panel 3(b). Simultaneously, in Fig. 3(d) the intensity of the SM is suppressed in that same detuning interval. Here, the master laser couples to the gain medium via injection into the WM and reduces the available gain for the SM.

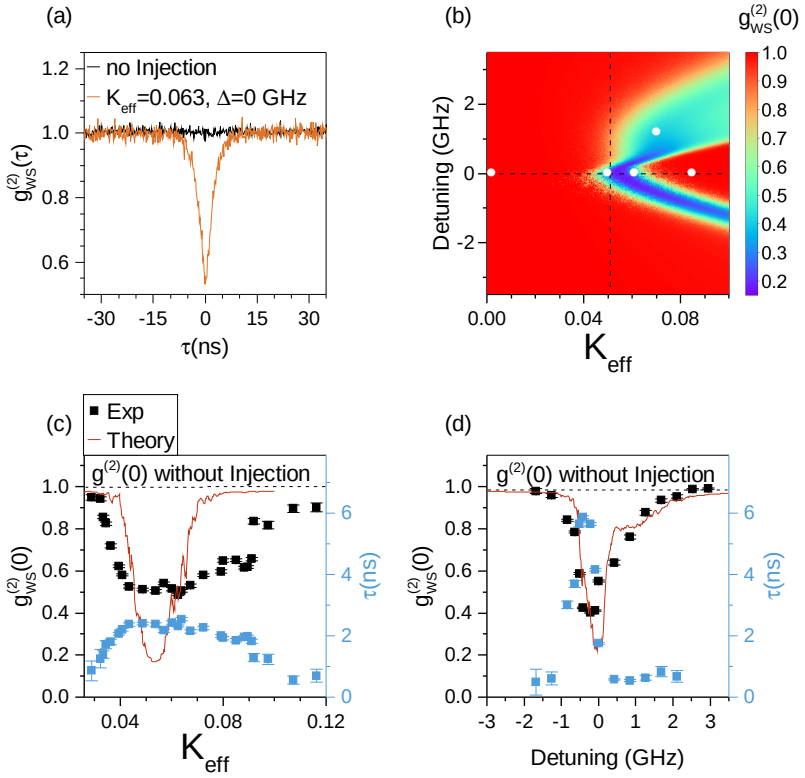

Fig. 4. (a) Exemplary experimental cross-correlation measurements $g^{(2)}_{\mathrm{WS}}(0)$ without injection (black curve) and with injection into the WM with $K_{\mathrm{eff}} = 0.063$. Pronounced anti-bunching reveals SM interaction and mode switching under optical injection. (b) Simulated $g^{(2)}_{\mathrm{WS}}(0)$ under variation of K_{eff} and detuning. Experimental and theoretical $g^{(2)}_{\mathrm{WS}}(0)$ and correlation time τ for driven K_{eff} (c) and detuning (d).

The gain coupling of orthogonally polarized modes of our bimodal microlaser is critical to understand the interplay of the modes under optical injection. More insight into the underlying dynamics is obtained by cross-correlation measurements between the two optical modes. It is known that in free-running microlasers, the two modes can exhibit stochastic switching which is identified by cross-correlating their intensity [39, 48] and it is interesting to study if this behavior

Optics EXPRESS

can be influenced and externally controlled by optical injection. For this purpose, the signal of the SM and the WM is split at the polarizing beam splitter in the detection path and is selectively forwarded to SPCMs after spectral selection via the two independent monochromators as can be seen in Fig. 1.

The intensity cross-correlation between SM and WM without injection is presented in Fig. 4(a), black curve. It shows values close to $g^{(2)}_{\mathrm{WS}}(0) = 1$, which indicates the absence of temporal correlations (and thus switching) of WM and SM emission. However, optical injection into the WM in the same conditions causes strong switching in the microlaser, as verified by the pronounced anti-bunching in the SM-WM cross-correlation of the orange curve in Fig. 4(a). Here, photon-anti-bunching verifies that simultaneous photon emission of both modes is strongly suppressed and indicates that the lasing action switches dynamically from the SM to the WM and vice versa under optical injection into the WM.

The simulations allow us to calculate a cross-correlation map under variation of the detuning and the effective coupling strength to obtain comprehensive insight into the injection induced mode interaction. The corresponding intensity cross-correlation between the SM and WM, $g^{(2)}_{\mathrm{WS}}(0)$, is presented in the 2D heatmap in Fig. 4(b), which allows us to identify regions of enhanced inter-mode correlation (blue and greenish areas). These regions correspond to the boundary regions of the locking cone in Fig. 2(d), where lasing of the weak mode is possible, but its dynamical stability against stochastic perturbations is very low. The numeric results further indicate the absence of temporal switching events between the SM and WM for small K_{eff} or large detuning. For large K_{eff} and low Δ is $g^{(2)}_{\mathrm{WS}}(0) \approx 1$, within the locking region and far from its stability boundaries, the powerful injection stabilizes the weak mode lasing state and thus suppresses switching events. Because of long integration times it is not feasible to experimentally reproduce the theoretically predicted cross-correlations of Fig. 4(b) in the full parameter range. Instead, we perform measurements along a horizontal and vertical cut through the 2D heatmap, as indicated by the black dashed lines in Fig. 4(b). The associated experimental results (dots) are plotted in panels 4(c) and 4(d) along with the theoretical data (red line).

A parameter scan along the horizontal dashed line in Fig. 4(b), i.e. $g^{(2)}_{\mathrm{WS}}(0)$ under variation of the injection strength K_{eff} for constant detuning $\Delta = 0$, reveals the onset of switching events between the SM and WM for K_{eff} exceeding ≈ 0.04. With increasing injection strength, $g^{(2)}_{\mathrm{WS}}(0)$ reaches a minimum of approximately 0.5 at $K_{\mathrm{eff}} \approx 0.05$ before it increases again towards unity. These results indicate that injection into the WM destabilizes lasing of the SM and leads to pronounced stochastic switching events at a ns time-scale as can be seen in the corresponding correlation times τ plotted in Fig. 4(c). The correlation time is linked to the dwell time which describes the residence time after a mode switch. With increasing injection strength into the WM, its lasing is stabilized while emission of SM is suppressed due to the gain competition. The simulation data shows the emergence of switching at the same injection strength, but with an overall narrower switching region width. Our simulation of the time dependent dynamics shows that indeed switching events are responsible for the low value of the $g^{(2)}_{\mathrm{WS}}(0)$. Both in experiment and simulations these regions of low $g^{(2)}_{\mathrm{WS}}(0)$ are found for positive detuning for the case of injection into the WM. Concurrent, the experimental correlation time depends strongly on the switching incidence and varies between hundreds of ps to 2.5 ns. We also studied the mode cross-correlation for a fixed injection strength as a function of detuning which is plotted in Fig. 4(d) and corresponds to a vertical cut through the 2D heatmap in Fig. 4(b). Here, the SM-WM switching events occur in a narrow range of 3 GHz around zero detuning. In this case, experiment and theory are in very good agreement and both indicate a sharp onset of switching for negative and a smoother one for positive Δ.

We plot the simulated time series of the intensity of both modes at different parameter values denoted by the white dots in Fig. 4(b). The time series in Fig. 5 clearly illustrate the effects

Optics EXPRESS

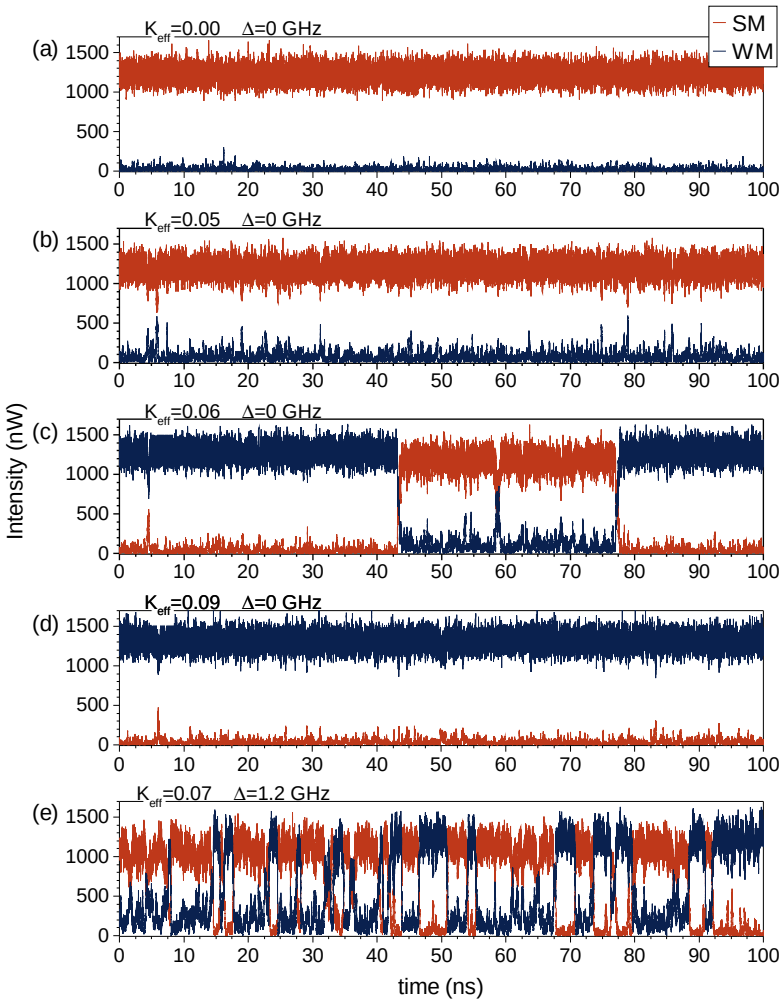

Fig. 5. Time series for injection into the WM with $\Delta = 0$ GHz and increasing injection strength. (a) $K_{\text{eff}} = 0$: While the SM is in a stable lasing mode, the WM shows low intensity and is well below the onset of lasing. (b) $K_{\text{eff}} = 0.05$: Both SM and WM fluctuate anti-correlated. (c) $K_{\text{eff}} = 0.06$: The WM is dominating and switching events occur. (d) $K_{\text{eff}} = 0.09$: The WM is stable lasing while the SM is dark. (e) $\Delta = 1.3$ GHz and $K_{\text{eff}} = 0.07$: SM and WM switch often for positive detuning.

Optics EXPRESS

of increasing injection in the non-lasing mode in panels 5(a)-5(d). We observe a transition from stable SM emission to stable WM emission, passing through instability regimes. Without injection for $K_{\mathrm{eff}} = 0$, the SM is lasing and switching processes do not occur. For small $K_{\mathrm{eff}} = 0.05$, anti-correlated fluctuations take place between the two modes with a duration of ~ 100 ps. Moreover, the average intensity of the WM is slightly increased, but still dominated by stochastic intensity spikes. At $K_{\mathrm{eff}} = 0.06$, the WM dominates and is most of the time in the lasing regime. However, the SM lasing state is still comparably stable, such that mode switching events on a time scale of several tens of ns can arise. We explain the occurrence of the switching events with the underlying deterministic anti-phase oscillations of both modes. In the lasing regime, the WM has a slightly higher average intensity than the SM due to the additional power provided by the injection signal. For even higher injection strength, the WM is continuously in the lasing regime while the SM is strongly suppressed and operates in the spontaneous emission regime below threshold. The parameter for Fig. 5(e) are chosen to be in the greenish area of Fig. 4(b) for positive detuning where enhanced switching is expected. On the time-scale of ns the SM and WM switch in intensity. The time series validate the assumption of stochastical mode switching induced by optical injection.

Noteworthy, lasers for applications in information processing are becoming smaller and smaller in interest of energy efficiency. The spontaneous emission gets a more important role in these devices and will lead to an enhanced impact of stochastic switching effects in micro- and nanolasers. If desired for applications, our results show that optical injection is a practical way to suppress stochastic polarization switching in such nanophotonic devices. Additionally, the truly random character is interesting for quantum-fluctuation based random number generation.

4. Conclusions

In conclusion, we have shown that optical injection in bimodal microlasers strongly influences the interrelation of the modes dynamics, majorly affecting the non-injected mode. While the injected mode locks on the master laser, the non-injected mode decreases in intensity because of gain competition between both modes. Optical injection in the non-lasing WM initiates stochastic switching or, with high injection strength, stabilizes lasing in the second mode. The switching dynamics are reflected experimentally in the emission spectra and cross correlation measurements which are in good agreement with the simulations. The numerical time series prove stochastical switching to be responsible for the low cross correlation values. Our studies push the limits of polarization resolved injection locking experiments towards the regime of ultra-low light levels in the sub-μW regime of cavity-enhanced microlaser. It has high potential to pave the way for future applications of micro- and nanolasers for instance in the fields of spin-injection lasers and photonic reservoir computing for which a precise tailoring of the birefringence and a deep understanding of the injection locking properties in the presence of high spontaneous emission noise is crucial.

Appendix A: Sample technology

The gain medium consists of a single layer of $In_{0.3}Ga_{0.7}As$ QDs with a $5 \cdot 10^9/\mathrm{cm}^2$ density. The QD layer is embedded in the field antinode of the central one-λ-thick GaAs cavity which is sandwiched between the bottom (top) distributed Bragg reflector consisting of 30 (26) alternating $\lambda/4$-thick AlAs/GaAs. Based on the planar cavity, electron beam lithography and plasma etching are used to realize high-Q micropillars with a diameter of 5 μm. Subsequently, the micropillars are planarized with benzocyclobutene and electrically contacted with ring gold contacts patterned by a second EBL process, see Fig. 1(b) for a schematic view of the device design. Detailed information on the sample processing can be found in [49].

The comparatively low volume (on the order of 5 $\mu\mathrm{m}^3$) and the high quality factor (Q of about 10.000) of the fabricated QD-micropillars lead to pronounced cQED effects. The most

Optics EXPRESS

Table 1. **Parameters used for the simulations if not stated otherwise.**

Fitted Parameters		**Value**
Optical cavity losses, strong (weak) mode	κ_s (κ_w)	78 (77) ns^{-1}
Optical gain coefficient, strong (weak) mode	g_s^0 (g_w^0)	11.15 (10.43) $\frac{m^2}{V^2 s}$
Self gain compression, strong (weak) mode	ε_{ss} (ε_{ww})	7 (8) $\cdot 10^{-10}$ $\frac{m^2}{AV}$
Cross gain compression, strong (weak) mode	ε_{sw} (ε_{ws})	20 (23) $\cdot 10^{-10}$ $\frac{m^2}{AV}$
Spontaneous emission factor	β	$3 \cdot 10^{-3}$
Parasitic currents	J_p	510 µA
Injection efficiency	η	$1.72 \cdot 10^{-3}$
Linewidth enhancement factor	α	1
Reservoir carrier lifetime	τ_r	1 ns
QD lifetime	τ_{sp}	67.5 ps
Given Parameters		**Value**
Effective scattering rate	S^{in}	$7 \cdot 10^{-15}$ m^{2}ps^{-1}
Lasing mode volume	V	5 µm^3
Effective lasing mode area	A	15 µm^2
Number of (in)active QDs	$Z^{\mathrm{QD}}_{(inact)}$	400 (940)
Background refractive index	n_{bg}	3.34
Photon energy	$\hbar\omega$	1.38 eV
	$\tilde{\varepsilon}$	$\varepsilon_0 n_{bg} c_0$

significant fingerprint of cQED is the efficient funneling of spontaneous emission into the cavity mode, strongly increasing the β-factor. This important parameter of microlasers is defined as the fraction of spontaneous emission that is emitted into the cavity mode. For the present devices with a diameter of 5 µm it is on the range of 10^{-3} – 10^{-2}, a value significantly higher than 10^{-4} – 10^{-6} achieved for standard VCSEL lasers based on a quantum well gain medium.

In the present bimodal micropillar laser is the fundamental cavity mode split into two orthogonally polarized modes with a spectral splitting of 47 µeV. The mode splitting is caused by small structural asymmetries in the pillar cross-section that arise during the patterning process [50], and possibly additional imperfections in the upper ring-shaped contact. The quality factors of the two modes are typically slightly different, so that also the gain coupling to each of those polarization-modes differs. This results in unequal gain/losses-ratios for the two modes and a characteristic input-output behavior with a dominating SM and an inferior WM [38] as we discuss in more detail in the section 3.

Optics EXPRESS

Appendix B: Theoretical model

The model used in this paper corresponds to the theoretical framework employed in [30]. We use a set of semi-classical stochastic rate equations, taking into account the electron scattering mechanisms into the QDs [51] with a minimal model as derived in our previous work [52]. We account for the two orthogonal linearly polarized micropillar modes by two separate complex electric field equations, denoted as weak mode and strong mode, corresponding to their respective output power above threshold. Neglecting spin-flip dynamics is required to model the behaviour in lower-β VCSEL devices [40], we instead couple both laser modes to a single charge-carrier type and describe the mode interaction by phenomenological gain compression terms. We model the electrical fields E_j of the two modes $j \in \{w, s\}$, the occupation probability of the active and inactive quantum dots $\rho_{\text{(in)act}}$, and the reservoir carrier density n_r. Here we denote as active the portion of QDs within the inhomogeneous distribution that couple to the lasing mode via stimulated emission.

$$\frac{\partial}{\partial t}E_j(t) = \left[\frac{\hbar\omega}{\epsilon_0\epsilon_{bg}}\frac{Z^{\text{QD}}}{V}g_j\big(2\rho(t)-1\big) - \kappa_j\right](1+i\alpha)E_j(t) + \frac{\partial}{\partial t}E_j\Big|_{\text{sp}} + \frac{\partial}{\partial t}E_j\Big|_{\text{inj}} \tag{1}$$

$$\frac{\partial}{\partial t}\rho_{\text{act}}(t) = -\sum_{j\in\{s,w\}} g_j\big[2\rho(t)-1\big]|E_j(t)|^2 - \frac{\rho(t)^2}{\tau_{\text{sp}}} + S^{in}n_r(t)\big[1-\rho(t)\big], \tag{2}$$

$$\frac{\partial}{\partial t}n_r(t) = \frac{\eta}{e_0 A}(J-J_p) - S^{in}n_r(t)\frac{2Z^{\text{QD}}}{A}\big[1-\rho(t)\big] - \frac{n_r(t)}{\tau_r} - \frac{2Z^{\text{QD}}_{\text{inact}}\rho_{\text{inact}}}{A\tau_{\text{sp}}}. \tag{3}$$

Carrier inversion in the QDs is achieved indirectly by applying a current J to the carrier reservoir n_r, from where electrons scatter into the QDs with the rate $S^{in} \times n_r(t)$. We include a pump-efficiency factor η as well as the parasitic pump current J_p to account for experimental current losses. Electrons may also be lost through spontaneous recombination, expressed through the carrier reservoir lifetime τ_r. Lastly, scattering into the inactive quantum dots is considered, whose occupation probability is assumed to correspond to the steady state of Eq. (2) without stimulated emission.

$$\rho_{\text{inact}}(t) = (\tau_{\text{sp}}S^{in}n_r(t))(1+\tau_{\text{sp}}S^{in}n_r(t))^{-1}. \tag{4}$$

Both electric field modes are assumed to interact with the same carrier population, as their respective frequencies only differ by a few GHz. This leads to gain competition between the modes, modeled by gain compression factors ε_{jk} in the gain term

$$g_j = g_j^0\left(1+\varepsilon_{js}\tilde{\varepsilon}|E_s(t)|^2 + \varepsilon_{jw}\tilde{\varepsilon}|E_w(t)|^2\right)^{-1}, \tag{5}$$

with $j \in w, s$. Therefore the gain g_j of both modes is reduced (compressed), if one mode exhibits large intensities. The stochastic nature of spontaneous emission is modeled via the noise term

$$\frac{\partial}{\partial t}E_j\Big|_{\text{sp}} = \sqrt{\beta\frac{\hbar\omega}{\epsilon_0\epsilon_{bg}}\frac{2Z^{\text{QD}}}{V}\frac{\rho_{\text{act}}^2}{\tau_{\text{sp}}}}\xi_j(t), \tag{6}$$

where $\xi(t) = \xi_1 + i\xi_2$ is a complex Gaussian white noise term, fulfilling

$$\langle\xi_i(t)\rangle = 0 \text{ and } \langle\xi_i(t_1)\xi_j(t_2)\rangle = \delta_{i,j}\delta(t_1-t_2). \tag{7}$$

The injection into the device is expressed by

$$\frac{\partial}{\partial t}E_j^{\text{inj}}(t) = K_j\kappa_j E_0\exp\left(2\pi i(\Delta\nu_{\text{inj}} - \nu_j^{(0)})t\right), \tag{8}$$

Optics EXPRESS

where E_0 is chosen as the averaged amplitude of the electric field inside the device for the chosen parameters,

$$E_0 = \sqrt{\langle |E_s|^2 \rangle + \langle |E_w|^2 \rangle}. \tag{9}$$

The free-running lasing frequency of the individual modes is given by $\nu_j^{(0)}$, such that for $\Delta\nu_{\mathrm{inj}} = 0$, the master laser is resonant with the respective micopillar laser mode. The initial values of the fitted parameters were taken from measurements of similar micropillar devices or from established values from previous publications [30, 37, 39, 53]. All parameters used in the simulations are listed in Table 1.

Funding

European Research Council (ERC) (615613); German Research Foundation (DFG) (CRC787, CRC910 and GRK1558, 404943123).

References

1. O. Painter, R. K. Lee, A. Scherer, A. Yariv, J. D. O'Brien, P. D. Dapkus, and I. Kim, "Two-dimensional photonic band-gap defect mode laser," Science **284**, 1819–1821 (1999).
2. S. Reitzenstein, A. Bazhenov, A. Gorbunov, C. Hofmann, S. Münch, A. Löffler, M. Kamp, J. P. Reithmaier, V. D. Kulakovskii, and A. Forchel, "Lasing in high-q quantum-dot micropillar cavities," Appl. Phys. Lett. **89**, 051107 (2006).
3. M. T. Hill, Y.-S. Oei, B. Smalbrugge, Y. Zhu, T. de Vries, P. J. van Veldhoven, F. W. M. van Otten, T. J. Eijkemans, J. S. P. Turkiewicz, H. de Waardt, E. J. Geluk, S.-H. Kwon, Y.-H. Lee, R. Nötzel, and M. K. Smit, "Lasing in metallic-coated nanocavities," Nat. Photonics (2007).
4. R. F. Oulton, V. J. Sorger, T. Zentgraf, R.-M. Ma, C. Gladden, L. Dai, G. Bartal, and X. Zhang, "Plasmon lasers at deep subwavelength scale," Nature **461**, 629 (2009).
5. W. W. Chow and S. Reitzenstein, "Quantum-optical influences in optoelectronics—an introduction," Appl. Phys. Rev. **5**, 041302 (2018).
6. H. Yokoyama, "Physics and device applications of optical microcavities," Science **256**, 66–70 (1992).
7. M. Nomura, N. Kumagai, S. Iwamoto, Y. Ota, and Y. Arakawa, "Laser oscillation in a strongly coupled single-quantum-dot-nanocavity system," Nat. Phys. **6**, 279–283 (2010).
8. M. Khajavikhan, A. Simic, M. Katz, J. H. Lee, B. Slutsky, A. Mizrahi, V. Lomakin, and Y. Fainman, "Thresholdless nanoscale coaxial lasers," Nature **482**, 204–207 (2012).
9. T. Wang, G. Puccioni, and G. Lippi, "Dynamical buildup of lasing in mesoscale devices," Sci. Rep. **5**, 15858 (2015).
10. K. J. Vahala, "Optical microcavities," Nature **424**, 839–846 (2003).
11. M. Lermer, N. Gregersen, F. Dunzer, S. Reitzenstein, S. Höfling, J. Mørk, L. Worschech, M. Kamp, and A. Forchel, "Bloch-wave engineering of quantum dot micropillars for cavity quantum electrodynamics experiments," Phys. Rev. Lett. **108**, 057402 (2012).
12. S. Kreinberg, T. Grbešić, M. Strauß, A. Carmele, M. Emmerling, C. Schneider, S. Höfling, X. Porte, and S. Reitzenstein, "Quantum-optical spectroscopy of a two-level system using an electrically driven micropillar laser as a resonant excitation source," Light. Sci. & Appl. **7** (2018).
13. S. Wieczorek, B. Krauskopf, T. B. Simpson, and D. Lenstra, "The dynamical complexity of optically injected semiconductor lasers," Phys. Rep. **416**, 1–128 (2005).
14. D. O'Shea, S. Osborne, N. Blackbeard, D. Goulding, B. Kelleher, and A. Amann, "Experimental classification of dynamical regimes in optically injected lasers," Opt. Express **22**, 21701–21710 (2014).
15. S. Meinecke, B. Lingnau, A. Röhm, and K. Lüdge, "Stability of optically injected two-state quantum-dot lasers," Ann. Phys. **529**, 1600279 (2017).
16. E. Viktorov, I. Dubinkin, N. Fedorov, T. Erneux, B. Tykalewicz, S. Hegarty, G. Huyet, D. Goulding, and B. Kelleher, "Injection-induced, tunable all-optical gating in a two-state quantum dot laser," Opt. Lett. **41**, 3555–3558 (2016).
17. S. Osborne, K. Buckley, A. Amann, and S. O'Brien, "All-optical memory based on the injection locking bistability of a two-color laser diode," Opt. Express **17**, 6293–6300 (2009).
18. T. Erneux and P. Glorieux, *Laser dynamics* (Cambridge University, 2010).
19. I. Gatare, M. Sciamanna, J. Buesa, H. Thienpont, and K. Panajotov, "Nonlinear dynamics accompanying polarization switching in vertical-cavity surface-emitting lasers with orthogonal optical injection," Appl. Phys. Lett. **88**, 101106 (2006).
20. F. Denis-le Coarer, A. Quirce, A. Valle, L. Pesquera, M. A. Rodríguez, K. Panajotov, and M. Sciamanna, "Attractor hopping between polarization dynamical states in a vertical-cavity surface-emitting laser subject to parallel optical injection," Phys. Rev. E **97**, 032201 (2018).

Optics EXPRESS

21. H. Lin, S. Ourari, T. Huang, A. Jha, A. Briggs, and N. Bigagli, "Photonic microwave generation in multimode vcsels subject to orthogonal optical injection," J. Opt. Soc. Am. B **34**, 2381–2389 (2017).
22. Y. D. Jeong, J. S. Cho, Y. H. Won, H. J. Lee, and H. Yoo, "All-optical flip-flop based on the bistability of injection locked fabry-perot laser diode," Opt. Express **14**, 4058–4063 (2006).
23. T. Mori, Y. Yamayoshi, and H. Kawaguchi, "Low-switching-energy and high-repetition-frequency all-optical flip-flop operations of a polarization bistable vertical-cavity surface-emitting laser," Appl. Phys. Lett. **88**, 10–13 (2006).
24. S. H. Lee, H. W. Jung, K. H. Kim, M. H. Lee, B. S. Yoo, J. Roh, and K. A. Shore, "1-GHz all-optical flip-flop operation of conventional cylindrical-shaped single-mode VCSELs under low-power optical injection," IEEE Photonic Tech. L. **22**, 1759–1761 (2010).
25. S. Reitzenstein, T. Heindel, C. Kistner, A. Rahimi-Iman, C. Schneider, S. Höfling, and A. Forchel, "Low threshold electrically pumped quantum dot-micropillar lasers," Appl. Phys. Lett. **93**, 061104 (2008).
26. A. Carmele, J. Kabuss, F. Schulze, S. Reitzenstein, and A. Knorr, "Single photon delayed feedback: A way to stabilize intrinsic quantum cavity electrodynamics," Phys. Rev. Lett. **110**, 013601 (2013).
27. S. M. Hein, F. Schulze, A. Carmele, and A. Knorr, "Optical feedback-enhanced photon entanglement from a biexciton cascade," Phys. Rev. Lett. **113**, 027401 (2014).
28. S. Walter, A. Nunnenkamp, and C. Bruder, "Quantum synchronization of two Van der Pol oscillators," Ann. Phys. **527**, 131–138 (2015).
29. N. Lörch, S. E. Nigg, A. Nunnenkamp, R. P. Tiwari, and C. Bruder, "Quantum synchronization blockade: Energy quantization hinders synchronization of identical oscillators," Phys. Rev. Lett. **118**, 243602 (2017).
30. S. Kreinberg, X. Porte, D. Schicke, B. Lingnau, C. Schneider, S. Höfling, I. Kanter, K. Lüdge, and S. Reitzenstein, "Mutual coupling and synchronization of optically coupled quantum-dot micropillar lasers at ultra-low light levels," Nat. Commun. **10**, 1539 (2019).
31. M. Lindemann, G. Xu, T. Pusch, R. Michalzik, M. R. Hofmann, I. Žutić, and N. C. Gerhardt, "Ultrafast spin-lasers," Nature **568**, 212 (2019).
32. P. Moser, J. A. Lott, G. Larisch, and D. Bimberg, "Impact of the oxide-aperture diameter on the energy efficiency, bandwidth, and temperature stability of 980-nm vcsels," J. Light. Technol. **33**, 825–831 (2014).
33. H. Altug, D. Englund, and J. Vučković, "Ultrafast photonic crystal nanocavity laser," Nat. Phys. **2**, 484 (2006).
34. D. Brunner and I. Fischer, "Reconfigurable semiconductor laser networks based on diffractive coupling," Opt. Lett. **40**, 3854–3857 (2015).
35. T. Heuser, J. Große, A. Kaganskiy, D. Brunner, and S. Reitzenstein, "Fabrication of dense diameter-tuned quantum dot micropillar arrays for applications in photonic information processing," APL Photonics **3**, 116103 (2018).
36. T. Heuser, J. Große, S. Holzinger, M. Sommer, and S. Reitzenstein, "Development of highly homogenous quantum dot micropillar arrays for optical reservoir computing," IEEE J. Sel. Top. Quant. pp. 1–3 (2019).
37. E. Schlottmann, S. Holzinger, B. Lingnau, K. Lüdge, C. Schneider, M. Kamp, S. Höfling, J. Wolters, and S. Reitzenstein, "Injection locking of quantum-dot microlasers operating in the few-photon regime," Phys. Rev. Appl. **6** (2016).
38. H. A. M. Leymann, C. Hopfmann, F. Albert, A. Foerster, M. Khanbekyan, C. Schneider, S. Höfling, A. Forchel, M. Kamp, J. Wiersig, and S. Reitzenstein, "Intensity fluctuations in bimodal micropillar lasers enhanced by quantum-dot gain competition," Phys. Rev. A **87**, 053819 (2013).
39. C. Redlich, B. Lingnau, S. Holzinger, E. Schlottmann, S. Kreinberg, C. Schneider, M. Kamp, S. Höfling, J. Wolters, S. Reitzenstein, and K. Lüdge, "Mode-switching induced super-thermal bunching in quantum-dot microlasers," New J. Phys. **18**, 063011 (2016).
40. M. Virte, K. Panajotov, H. Thienpont, and M. Sciamanna, "Deterministic polarization chaos from a laser diode," Nat. Photonics **7**, 1–6 (2013).
41. M. C. Soriano, J. García-Ojalvo, C. R. Mirasso, and I. Fischer, "Complex photonics: Dynamics and applications of delay-coupled semiconductors lasers," Rev. Mod. Phys. **85**, 421 (2013).
42. A. Uchida, K. Amano, M. Inoue, K. Hirano, S. Naito, H. Someya, I. Oowada, T. Kurashige, M. Shiki, S. Yoshimori, K. Yoshimura, and P. Davis, "Fast physical random bit generation with chaotic semiconductor lasers," Nat. Photonics **2**, 728 (2008).
43. F. Rogister, A. Locquet, D. Pieroux, M. Sciamanna, O. Deparis, P. Mégret, and M. Blondel, "Secure communication scheme using chaotic laser diodes subject to incoherent optical feedback and incoherent optical injection," Opt. Lett. **26**, 1486–1488 (2001).
44. M. Sciamanna and K. A. Shore, "Physics and applications of laser diode chaos," Nat. Photonics **9**, 151 (2015).
45. G. Björk, A. Karlsson, and Y. Yamamoto, "Definition of a laser threshold," Phys. Rev. A **50**, 1675–1680 (1994).
46. Z. G. Pan, S. Jiang, M. Dagenais, R. A. Morgan, K. Kojima, M. T. Asom, R. E. Leibenguth, G. D. Guth, and M. W. Focht, "Optical injection induced polarization bistability in vertical-cavity surface-emitting lasers," Appl. Phys. Lett. **63**, 2999–3001 (1993).
47. B. Lingnau, W. W. Chow, and K. Lüdge, "Amplitude-phase coupling and chirp in quantum-dot lasers: influence of charge carrier scattering dynamics," Opt. Express **22**, 4867–4879 (2014).
48. M. Marconi, J. Javaloyes, P. Hamel, F. Raineri, A. Levenson, and A. M. Yacomotti, "Far-from-equilibrium route to superthermal light in bimodal nanolasers," Phys. Rev. X **8**, 011013 (2018).
49. C. Böckler, S. Reitzenstein, C. Kistner, R. Debusmann, A. Löffler, T. Kida, S. Höfling, A. Forchel, L. Grenouillet, J. Claudon, and J. M. Gérard, "Electrically driven high-q quantum dot-micropillar cavities," Appl. Phys. Lett. **92**, 091107 (2008).

Optics EXPRESS

50. S. Reitzenstein, C. Hofmann, A. Gorbunov, M. Strauß, S. H. Kwon, C. Schneider, A. Löffler, S. Höfling, M. Kamp, and A. Forchel, "AIAs/GaAs micropillar cavities with quality factors exceeding 150.000," Appl. Phys. Lett. **90**, 1–4 (2007).
51. K. Lüdge and E. Schöll, "Quantum-dot lasers – desynchronized nonlinear dynamics of electrons and holes," IEEE J. Quantum Elect. **45**, 1396–1403 (2009).
52. B. Lingnau and K. Lüdge, "Analytic characterization of the dynamic regimes of quantum-dot lasers," Photonics **2**, 402–413 (2015).
53. M. Virte, K. Panajotov, and M. Sciamanna, "Bifurcation to nonlinear polarization dynamics and chaos in vertical-cavity surface-emitting lasers," Phys. Rev. A **87**, 013834 (2013).